Numerical solutions to a kinetic model for the plasma-sheath problem with charge exchange collisions of ions

Z. Sternovsky, K. Downum, and S. Robertson
Department of Physics, University of Colorado, Boulder, Colorado 80309-0390, USA
(Received 6 January 2004; published 31 August 2004)

A kinetic model of the plasma-sheath problem is presented that includes the effects of charge-exchange collisions of the ion. The collisions are modeled as a sink for accelerated ions and as a source of cold ions. Solutions are obtained by numerical integration of Poisson's equation from a point near the plasma midplane to the wall. In the quasineutral region, these solutions agree with earlier analytic work. As the mean free path is decreased, the current density at the wall decreases and the potential profile in the quasineutral region shows a smooth transition from a parabolic profile to a nearly cubic profile determined by the ion mobility. An approximate expression is found for the ion flux to the wall in the collisional limit.

DOI: 10.1103/PhysRevE.70.026408 PACS number(s): 52.40.Kh

I. INTRODUCTION

In many laboratory plasmas the shortest mean free path is the one for charge exchange collisions of ions. This mean free path is often smaller than the dimensions of the plasma but greater than the dimensions of the sheath. In this case the bulk of the plasma should be modeled by equations that include the effects of collisions. Riemann [1] added charge-exchange collisions to the kinetic model of Tonks and Langmuir [2] and obtained an analytic solution for the quasineutral region. Riemann has also discussed in some detail the effects of ion collisions on fluid models of the sheath region [3]. Monte Carlo collisions of ions have been implemented in particle-in-cell codes [4], and these have been used to obtain the distribution function of ions hitting the wall [5]. For collisionless plasmas, Harrison and Thomson [6] obtained an analytic solution to the kinetic model valid in the quasineutral region. Self [7] obtained numerical solutions for the collisionless case valid from the midplane to the wall.

In this work, the kinetic model [2] is modified to include charge-exchange collisions. The numerical solutions presented here extend the collisional solution obtained by Riemann [1] from the quasineutral region to the wall for the case of a homogeneous source of ionization. The collisions are found to reduce the current density at the wall to a value significantly below the usual ion saturation current. Solutions are also found for the energy distribution of ions hitting the wall. This distribution is important in plasma processing applications [5] and in determining plasma-wall interactions in fusion devices [8,9].

In Sec. II we present a kinetic model with two source terms for ions. The first term describes homogeneous generation of cold ions that could occur from energetic electrons. The flux of these ions is attenuated with distance as a result of collisions characterized by a constant mean free path. There is a second source term for cold ions that is equal to the rate of loss of ions to these collisions. At each location the ion density is found by integration of the upstream sources. The electron density is modeled by the Boltzmann relation. An alternate version of the model in which individual ions are followed is presented briefly. A set of dimensionless units is introduced and the boundary conditions at the midplane are derived. In Sec. III, Poisson's equation is numerically integrated from a point near the midplane to the wall. Solutions are obtained for a range of mean free paths that is longer and shorter than the dimensions of the plasma. In the limit of short mean free path, the solutions in the quasineutral region are shown to agree with a collisional model based upon ion mobility. Section IV is a summary and conclusion.

II. MODELS

A homogeneous source of ionization R_0 is assumed in a region from $-L$ to $+L$. The continuity equation then requires that the particle flux of ions toward the wall be $J_{net}(x)=R_0x$, where x is measured from the midplane. The charge-exchange collisions of ions with cold neutrals are assumed to be characterized by a constant cross section and thus a constant mean free path $\lambda_{mfp}=1/n_n\sigma$, where n_n is the neutral density and σ is the collision cross section. The model makes use of the fact that these collisions do not change the value of J_{net}. The ions created by impact ionization or by charge exchange are assumed to be born at rest. This approximation is valid for most laboratory plasmas because the initial ion energy is much less than the potential through which they are subsequently accelerated.

A. Kinetic model

The differential contribution $dJ_0(x,\xi)$ to the particle flux at x from particles created at ξ by ionization is

$$dJ_0(x,\xi) = R_0\exp[-(x-\xi)/\lambda_{mfp}]d\xi, \tag{1}$$

where $x>\xi$ is assumed. The contribution of these ions to the density at x is found by dividing their current contribution by their velocity $v(x,\xi)$ determined from energy conservation to obtain

$$dn_{i,0}(x) = \frac{dJ_0(x,\xi)}{v(x,\xi)} = \frac{R_0 \exp[-(x-\xi)/\lambda_{mfp}]}{\left[\frac{2q}{m_i}[\Phi(\xi)-\Phi(x)]\right]^{1/2}} d\xi, \quad (2)$$

where q is the elementary charge, m_i is the ion mass, $\Phi(x)$ is the space potential, and the subscript zero refers to ions created by impact ionization of neutrals.

Those ions lost in charge-exchange collisions create an equal number of new ions beginning at zero velocity. Thus, there is a second source term, R_{cx}, that is equal to the number of charge-exchange collisions per unit volume. The net flux passing through a distance $d\xi$ creates collisions at the rate $R_{cx}=J_{net}/\lambda_{mfp}=R_0\xi/\lambda_{mfp}$. These contribute a second term to the density at x

$$dn_{i,cx}(x) = \frac{R_{cx} \exp[-(x-\xi)/\lambda_{mfp}]}{\left[\frac{2q}{m_i}[\Phi(\xi)-\Phi(x)]\right]^{1/2}} d\xi, \quad (3)$$

where the subscript cx refers to the ions created by charge-exchange collisions. The total ion density $n_i(x)$ is then found from the integral of the sum of the two differential values for n_i:

$$n_i(x) = \int_0^x \frac{R_0(1+\xi/\lambda_{mfp})\exp[-(x-\xi)/\lambda_{mfp}]}{\left[\frac{2q}{m_i}[\Phi(\xi)-\Phi(x)]\right]^{1/2}} d\xi. \quad (4)$$

This model is similar to the kinetic model with charge-exchange collisions examined analytically in the quasineutral region by Riemann [1]. The potential profile is found by integration of Poisson's equation,

$$\frac{\varepsilon_0}{q}\frac{d^2\Phi(x)}{dx^2} = n_0 \exp[q\Phi(x)/T_e] - n_i(x), \quad (5)$$

where n_0 is the plasma density at the midplane, and T_e is the electron temperature in energy units.

Homogeneous ionization has been assumed for simplicity and clarity; however, the model can be easily modified for the case of ionization proportional to the local electron density or to the neutral gas density. This is done by defining $J(x)$ as the integral from 0 to x of $R(\xi)=Cn_n(\xi)n_e(\xi)$, where n_e is the electron density and C is a constant.

B. Particle model

An alternate numerical model was developed in which individual ions are followed. In the usual particle-in-cell code, the ion equations of motion are advanced in time and Poisson's equation is solved at each time step to update the potential profile. In the problem that is addressed here, the ions move only in the positive x direction and thus the ion density at x is determined only by conditions between x and the midplane. In principle, the problem can be solved by integration along the spatial coordinate in "one pass" if both Poisson's equation and the ions are advanced simultaneously in x. In practice, this approach has two problems. The first is that the ion density near the midplane is calculated from a small subset of particles; thus, fluctuations are relatively large. The effect of the fluctuations is reduced by finding the polynomial expression for $\Phi(x)$ that gives the least error in Poisson's equation in an initializing region near the midplane. In addition, the charge density fluctuations are reduced by having the ions created uniformly in space rather than at random locations. The second problem is that each particle moves to each downstream grid point; thus, the ion number density is not simply related to the density of ion locations. This problem is solved by finding the density with the same method that is used in the kinetic model.

One computational ion is generated per grid point and the flux associated with each ion is $R_0\Delta\xi$, where $\Delta\xi$ is the grid spacing chosen to be much smaller than the Debye length λ_D. The density associated with this ion is obtained from the current contribution divided by the ion velocity. The density contributions of the ions born upstream are summed to obtain the ion density

$$n_i(x_k) = \sum_{i=0}^{k} \frac{R_0\Delta\xi}{v_{i,k}}, \quad (6)$$

where the sum is taken over each ion born between 0 and x_k, and $v_{i,k}$ is the velocity of the ith ion evaluated at x_k. The details of the procedure to find the velocity and the density with sufficient accuracy are described in the Appendix. The birth of the ion can be due to ionization or a charge-exchange collision. The collisions are modeled with a Monte Carlo method.

The particle model does not require integration of the equations of motion for the ions. It is only necessary to evaluate the sum in Eq. (6). The model has the advantage that more complicated collision models can be implemented, as long as these do not result in ions with negative velocities. For example, the addition of angular scattering to the collision model would allow the spread in angles of incidence to be determined at the wall, which is important in plasma processing applications.

C. Boundary conditions at the midplane

The equations are solved in a dimensionless form with $\tilde{x}=x/\lambda_D$, $\lambda_D=(\varepsilon_0 T_e/n_0 q^2)^{1/2}$, $\tilde{n}=n/n_0$, $\tilde{\Phi}=q\Phi/T_e$, $\tilde{u}=u/c_s$, $c_s=(T_e/m_i)^{1/2}$, $\lambda_{mfp}=1/n_n\sigma$, $\tilde{\lambda}_{mfp}=\lambda_{mfp}/\lambda_D$, and $\tilde{R}_0=R_0\lambda_D/n_0 c_s$. The boundary conditions near the midplane are found using a power series expansion for the potential with the plasma potential set to zero

$$\tilde{\Phi}(\tilde{x}) \cong -\alpha\tilde{x}^2 - \beta\alpha^{3/2}\tilde{x}^3 - \gamma(\alpha\tilde{x}^2)^2, \quad (7)$$

where α, β, and γ are to be determined. The coefficient α will be shown to be proportional to the inverse of the square of the length scale L; thus, the series is in powers of x/L. The solution must be symmetric about the midplane; thus, the cubic term must be interpreted as the third power of the absolute value of x.

Using only the lowest order term in the expansion, $\tilde{\Phi}(\tilde{x}) \cong -\alpha\tilde{x}^2$, and $\lambda_{mfp}\to\infty$, one finds after substituting into Eq. (4) and integration that the ion density close to the midplane is

$$\tilde{n}_i(0) \cong \frac{\pi \tilde{R}_0}{\sqrt{8\alpha}}. \tag{8}$$

For points near the origin, $\tilde{n}_e(\tilde{x})=1$ may be assumed. Using the lowest order term for the potential in Poisson's equation, $d^2\tilde{\Phi}/d\tilde{x}^2=\tilde{n}_e-\tilde{n}_i$, it is found that $\tilde{n}_i(0)=1+2\alpha$. From this relation and Eq. (8).

$$\tilde{R}_0 = \frac{\sqrt{8\alpha}}{\pi}(1+2\alpha), \tag{9}$$

which defines the coefficient α in terms of the source rate $\tilde{R}_0$. The particle flux at the wall is approximately 0.50 in dimensionless units, [7]; thus, the approximate distance from the midplane to the wall is $\tilde{x}_w \approx L/\lambda_D \approx 0.5/\tilde{R}_0 \approx \pi/\sqrt{32\alpha}$. This applies only to the collisionless case. The difference between the electron and ion densities that drives the solution to Poisson's equation is 2α in dimensionless units. This is a small quantity, of order $(\lambda_D/L)^2$; thus, great accuracy is needed in evaluating the integral for n_i in Eq. (4). This integral is converted to a sum over grid point intervals as described in the Appendix. It is necessary to start the integration of Poisson's equation many grid points from the origin in order to have enough terms in the sum for accurate values of n_i. An initializing interval ending at $\tilde{x}=0.15L/\lambda_D$ is found to be the shortest interval that consistently gives numerical stability.

The values of $\tilde{\Phi}(\tilde{x})$ on the initializing interval are assigned using the polynomial in Eq. (7). The first coefficient α is related to $\tilde{R}_0$ through Eq. (9). The coefficients β and γ are found by minimizing the error in Poisson's equation. A standard numerical routine that minimizes the sum of the mean square errors is applied to Poisson's equation on the initializing interval. In the collisionless case, the error is minimized with $\beta=0$ and $\gamma=1.37\pm0.03$ for α values from 5×10^{-4} to 5×10^{-8}, which correspond to a range of L from $\sim$25 to $\sim$2500 Debye length. This shows that γ has a universal value for the collisionless case and that the profile is nearly parabolic in the initializing region.

In the collisional case, the cubic term becomes larger as the mean free path is made shorter. The cubic dependence of Φ upon x can be seen by examining the ion mobility. Wannier [10,11] has shown that for charge-exchange collisions with a constant mean free path, the ion drift velocity is given by

$$\tilde{u} = \sqrt{2\tilde{E}\tilde{\lambda}_{mfp}/\pi}, \tag{10}$$

where $\tilde{E}=qE\lambda_D/T_e$. This result, also obtained by Smirnov [12] and by Riemann [1], is obtained simply by averaging the drift speeds over the exponential distribution of free paths. This result applies when the energy gained between collisions, $qE\lambda_{mfp}$, is much greater than the initial ion thermal energy, which is usually the case in both the quasineutral regions and sheaths. Ion mobilities for smaller electric fields may be calculated using a collision frequency that is velocity dependent [13].

Near the midplane, the ion flux is given by $\tilde{R}_0\tilde{x}$, the density is near unity, and thus the drift velocity $\tilde{u}$ must grow approximately linearly with $\tilde{x}$

$$\tilde{u}(\tilde{x}) \cong \frac{\tilde{R}_0\tilde{x}}{\tilde{n}_i(\tilde{x})}. \tag{11}$$

From Eqs. (10) and (11) and $\tilde{n}_i(\tilde{x})=1$, $\tilde{E}(\tilde{x})$ can be found and integrated once to obtain

$$\tilde{\Phi}(\tilde{x}) = -\frac{4(\alpha\tilde{x}^2)^{3/2}}{3\pi\tilde{\lambda}_{mfp}\sqrt{\alpha}}, \tag{12}$$

which is valid only near the midplane. This determines in the collisional limit a value for the polynomial coefficient in Eq. (7)

$$\beta_{calc} = \frac{4}{3\pi\tilde{\lambda}_{mfp}\sqrt{\alpha}} = \frac{8\sqrt{2}}{3\pi^2}\frac{1}{\tilde{R}_0\tilde{\lambda}_{mfp}}. \tag{13}$$

The high-field drift velocity, Eq. (10), is derived with the assumption that E changes negligibly in a mean free path; thus, Eq. (13) is expected to hold only for plasmas that have many collisions within the bulk plasma. Riemann [1] used the plasma approximation, $\tilde{n}_i(\tilde{x})=\exp[\Phi(\tilde{x})]$, with Eqs. (10) and (11) to obtain an approximate solution for the potential profile in the quasineutral region in the collisional case

$$\tilde{\Phi}(\tilde{x}) \cong \frac{1}{2}\ln\left[1-\frac{\pi\tilde{R}_0^2\tilde{x}^3}{3\tilde{\lambda}_{mfp}}\right]. \tag{14}$$

This function, when expanded as a polynomial, has a coefficient for the cubic term that is equal to β_{calc}.

The derivative of Eq. (14) gives the electric field in the quasineutral approximation

$$\tilde{E}(\tilde{x}) \cong \left(\frac{3}{2}\right)\frac{(\pi\tilde{R}_0^2/3\tilde{\lambda}_{mfp})\tilde{x}^2}{1-(\pi\tilde{R}_0^2/3\tilde{\lambda}_{mfp})\tilde{x}^3}. \tag{15}$$

As discussed later, the quasineutrality condition holds at least to the point where $\tilde{\Phi}=-0.5$ for large plasmas. Thus, we may use Eq. (14) to find the point $\tilde{x}_{0.5}$ where $\tilde{\Phi}=-0.5$

$$\tilde{x}_{0.5} = \left\{\frac{3\tilde{\lambda}_{mfp}[1-\exp(-1)]}{\pi\tilde{R}_0^2}\right\}^{1/3}, \tag{16}$$

and $\tilde{x}_{0.5}$ may be placed in Eq. (15) to obtain the electric field at this point,

$$\tilde{E}_{0.5} = \frac{2.58}{\tilde{x}_{0.5}}, \tag{17}$$

which is independent of the mean free path. The mobility, Eq. (10), may then be used to find the drift velocity, and from the density at this point, $\tilde{n}_i(\tilde{x}_{0.5})=0.607$, the ion flux can be found:

$$\tilde{J}_{0.5} = 0.607\sqrt{2\tilde{E}_{0.5}\tilde{\lambda}_{mfp}/\pi} \cong 0.778\left[\frac{\tilde{\lambda}_{mfp}}{\tilde{x}_{0.5}}\right] \cong 0.778\left[\frac{\lambda_{mfp}}{L}\right]. \tag{18}$$

The wall location $\tilde{x}_w$ is defined here as the location for which the ion and electron fluxes are equal. The electron flux in dimensionless units for a Maxwellian distribution is

$$\tilde{J}_e(\tilde{x}) = \sqrt{\frac{m_i}{2\pi m_e}}\exp[\tilde{\Phi}(\tilde{x})], \tag{19}$$

where m_e is the electron mass. For the collisionless case and in the limit of large plasma, $L/\lambda_D \to \infty$, the ion flux to the wall is $\tilde{J}=0.487$ [7]; thus, $\tilde{\Phi}(\tilde{x}_w)=-3.56$ for an electron-proton plasma. It is shown below that this potential becomes more negative for collisional plasmas.

The energy distribution of ions reaching the wall can be calculated from the relation

$$F(\tilde{W})d\tilde{W} = \tilde{R}_0[1+\xi(\tilde{W})/\tilde{\lambda}_{mfp}]\exp\left[-\frac{\tilde{x}_w-\xi(\tilde{W})}{\tilde{\lambda}_{mfp}}\right]d\xi, \tag{20}$$

where $\tilde{W}$ is the dimensionless ion energy and $\xi(\tilde{W})$ is the inverse function to $\tilde{W}(\xi)=\tilde{\Phi}(\xi)-\tilde{\Phi}(\tilde{x}_w)$. This may be rewritten as

$$F(\tilde{W}) = \tilde{R}_0[1+\xi(\tilde{W})/\tilde{\lambda}_{mfp}]\exp\left[-\frac{\tilde{x}_w-\xi(\tilde{W})}{\tilde{\lambda}_{mfp}}\right] \times\left[\left.\frac{d\tilde{\Phi}(\xi)}{d\xi}\right|_{\xi(\tilde{W})}\right]^{-1}. \tag{21}$$

III. NUMERICAL SOLUTIONS

A. Solutions in the collisionless case

The numerical model is applied to collisionless plasmas by simply taking $\lambda_{mfp}\to\infty$, and in this limit the model is the same as that investigated by Self [7]. Figure 1 is a plot of $\tilde{\Phi}(\tilde{x})$ from the midplane to the wall for a range of values of α. The analytic quasineutral solution of Harrison and Thompson [6] is also plotted. The numerical solutions approach the analytic solution with decreasing α (increasing plasma size L). Table I shows values for the distance $\tilde{x}$, the ion flux $\tilde{J}=\tilde{R}_0\tilde{x}$, the electric field $\tilde{E}$, and the ion density $\tilde{n}_i$ evaluated at the location for which $\tilde{\Phi}(\tilde{x})=-0.854$. This location is often taken as the sheath edge because the quasineutral solution [6] breaks down and gives $\tilde{E}$ infinitely large at this distance. At this point, the dimensionless ion flux asymptotically approaches 0.487 with increasing plasma size. This value is in agreement with Harrison and Thompson [6] and Self [7]. Table I also shows parameters evaluated at the wall, where the electron and ion fluxes are equalized assuming an electron-proton plasma. The slightly higher ion flux at the wall is due to the ion generation within the sheath region. In fluid models, the location where the fluid velocity becomes unity is used as a definition of the presheath-sheath boundary. In kinetic models, the fluid velocity is not a variable; thus, Table I does not include parameters at this location.

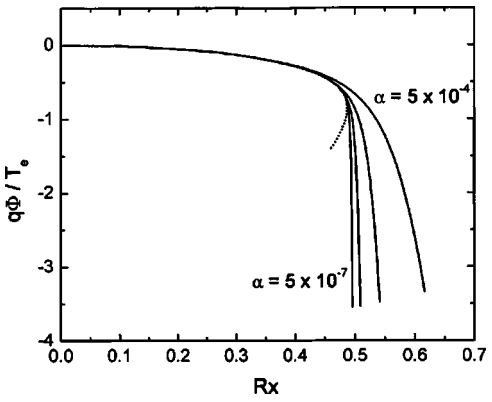

FIG. 1. The potential profiles for the collisionless case as a function of normalized distance for a range of α values ($5\times10^{-4}, 5\times10^{-5}, 5\times10^{-6}$, and 5×10^{-7}). The dotted line is the potential profile in the quasineutral approximation from Ref. [6].

Examination of Fig. 1 shows that Harrison and Thomson's analytic solution for the quasineutral region is valid for all values of L to approximately the point where $\tilde{\Phi}(\tilde{x})=-0.5$. The values of the other parameters at this location are listed in Table II. For plasmas with $L \geqslant 200\,\lambda_D$, $\tilde{J}$ and $\tilde{n}_i$ have reached their asymptotic values of 0.461 and 0.607, respectively. The electric field decreases approximately inversely with plasma size and approaches $\tilde{E}=2.64/\tilde{x}_{0.5}$. For sufficiently large plasmas, these values could be used to start the integration of Poisson's equation, Eq. (5).

TABLE I. Computed parameters obtained in the collisionless case.

		Values at $\tilde{\Phi}=-0.854$				Values at the wall				
α	$\pi/\sqrt{32\alpha}$	$\tilde{x}$	$\tilde{J}$	$\tilde{E}$	$\tilde{n}$	$-\tilde{\Phi}$	$\tilde{x}$	$\tilde{J}$	$\tilde{E}$	$\tilde{n}_i$
5×10^{-4}	24.8	25.9	0.521	0.26	0.502	3.33	30.48	0.615	1.00	0.276
5×10^{-5}	78.5	78.4	0.499	0.11	0.460	3.45	84.98	0.541	0.88	0.223
5×10^{-6}	248	244	0.491	0.062	0.442	3.52	252.8	0.509	0.82	0.200
5×10^{-7}	785	767	0.488	0.033	0.433	3.54	778.5	0.496	0.79	0.192
5×10^{-8}	2484	2422	0.487	0.018	0.429	3.55	2436	0.490	0.78	0.189

TABLE II. Computed parameters for the collisionless case at the distance for which $\tilde{\Phi}=-0.5$.

	$\tilde{\Phi}=-0.5$				
α	$\tilde{x}$	$\tilde{J}=\tilde{R}\tilde{x}$	$\tilde{E}$	$\tilde{n}_i$	$\tilde{x}\tilde{E}$
5×10^{-4}	23.3	0.470	0.091	0.631	2.14
5×10^{-5}	72.7	0.463	0.034	0.611	2.50
5×10^{-6}	229	0.461	0.011	0.607	2.61
5×10^{-7}	724	0.461	0.0036	0.607	2.63
5×10^{-8}	2292	0.461	0.0011	0.607	2.64

B. Solutions for finite mean free path

The collisional case is investigated in detail for a single plasma size, 252 λ_D, that corresponds to $\alpha=5\times10^{-6}$ in the collisionless case. Solutions are obtained for $\tilde{\lambda}_{mfp}=\infty$, 200, 100, 50, 20, 10, and 5 Debye lengths. The first of these values is to produce a collisionless case for comparison using the collisional version of the equations. The number of mean free paths within the plasma thus varies from ~0 to 50. The integration is performed from the end of the initializing region to the point $\tilde{x}_w$, where the electron and ion fluxes are equal. The ionization rate $\tilde{R}_0$ is adjusted, by trial and error, to hold constant the plasma size. Without this adjustment, the plasmas are different in extent, which makes comparisons less direct. This procedure is analogous to an experiment of fixed size in which the ionization rate is adjusted to give a constant plasma density as the mean free path is changed through varying the neutral gas pressure. Table III shows the calculated parameters. The value of $\tilde{E}$ at the wall is only weakly dependent upon λ_{mfp}. The ion flux at the wall (and thus the required ionization rate) falls by nearly a factor of 4 as λ_{mfp} is decreased to 5 λ_D. Figure 2 shows the collisional ion flux to the wall relative to the collisionless flux as a function of the mean free path. Figure 3 shows, from a separate set of calculations, that the ion flux does not change if the dimensionless plasma size, L/λ_D, is varied with $L/\lambda_{mfp}=10$. This indicates that L/λ_{mfp} is the controlling parameter.

The computed profiles of the potential for three different values of the mean free path are plotted together in Fig. 4. The change in the profile caused by reducing the mean free path is the rounding of the knee region. The values of the coefficient β in the initializing region obtained from the fitting routine are listed in Table III along with the value β_{calc} obtained from the analytic solution. There is good agreement at all values of the mean free path. The part of the curve in the quasineutral region is compared with the analytic solution in Fig. 5 for the shortest mean free path investigated. The calculated potential falls slightly more rapidly than the analytic solution from Eq. (14). The disagreement becomes greater in the less collisional cases with longer mean free paths. The discrepancy is because the mobility drift speeds in the plasma will be slightly lower than the Wannier value, Eq. (10), which applies only to uniform electric fields. The electric field increases with distance and the potential drop that determines the velocity is slightly less than that calculated from the local value of the electric field. The electric field necessary to remove the ions is thus slightly greater than determined by Eq. (9).

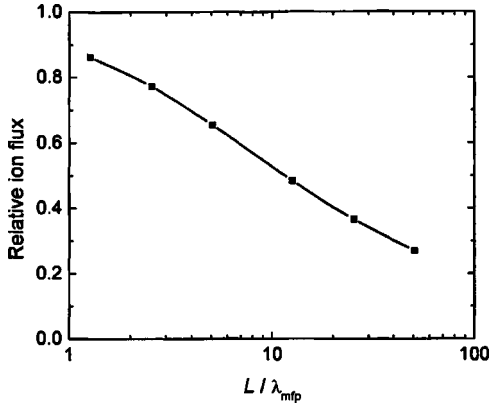

FIG. 2. The ion flux reduction at the wall due to collisions relative to the collisionless case for a constant plasma size $L=252.8\ \lambda_D$.

The accuracy of the simple analytic model for the quasineutral region is examined in Table IV. The values of the parameters from the numerical model at the point where $\tilde{\Phi}=-0.5$ are listed along with the parameters from analytic model, Eqs. (16)–(18). As the mean free path is decreased, the values of $\tilde{x}_{0.5}$, $\tilde{E}_{0.5}$, and $\tilde{J}_{0.5}$ from the analytic model approach to within a few percent of those from the numerical model. The relative distance from $\tilde{x}_{0.5}$ to $\tilde{x}_w$ in the collisional

TABLE III. Computed parameters at the wall from the collisional model. The ionization rate is adjusted to have constant plasma size of $\tilde{x}_w=252.8\lambda_D$. The first value of β is the value fitted in the initializing region and the second value is β_{calc} from Eq. (13).

λ_{mfp}	$\tilde{R}_0\times10^3$	β/β_{calc}	γ	$-\tilde{\Phi}$	$\tilde{J}$	$\tilde{E}$	$\tilde{n}_i$
∞	2.01	0/0	1.37	3.52	0.509	0.82	0.200
200	1.74	0.95/1.10	1.69	3.66	0.439	0.78	0.177
100	1.55	2.46/2.46	1.90	3.77	0.393	0.76	0.163
50	1.32	5.83/5.81	2.00	3.94	0.333	0.73	0.145
20	0.973	19.6/19.6	3.17	4.24	0.246	0.71	0.122
10	0.737	51.5/51.8	8.03	4.52	0.186	0.70	0.109
5	0.543	140.1/140.8	10.1	4.83	0.137	0.70	0.101

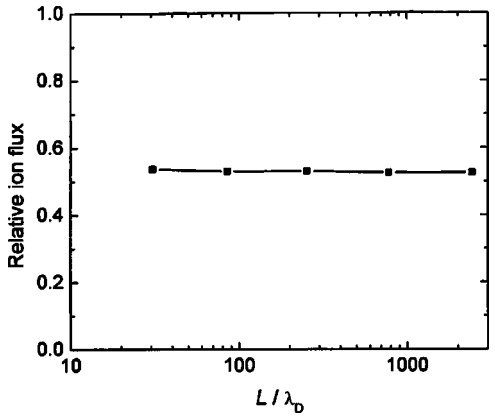

FIG. 3. The ion flux at the wall relative to the collisionless flux for constant $L/\lambda_{mfp}=10$.

case is plotted in Fig. 6 for a range of values of $\tilde{x}_w$. This distance may be used to calculate the additional current $(\tilde{x}_w - \tilde{x}_{0.5})\tilde{R}_0$ generated between $\tilde{x}_{0.5}$ and $\tilde{x}_w$. Examination of Table IV shows that this distance is a weak function of the mean free path.

The energy distribution of ions hitting the wall is plotted in Fig. 7(A). The energy distribution is peaked at $\tilde{\Phi}(\tilde{x}_w)$ in the limit of long mean free path. The distribution becomes more uniform as the mean free path is reduced. The greatest part of the potential drop occurs within about 40 Debye lengths of the wall; thus, the majority of ions will have fallen through a potential near to the wall potential unless the mean free path is shorter than $\sim 40\ \lambda_D$. In this case the highest energy ions are so strongly attenuated that they are missing from the distribution.

Energy distributions were also obtained using the particle model described in Sec. II B. The distribution for the case $\tilde{\lambda}_{mfp}=10$ is plotted in Fig. 7(B) along with the result from the kinetic model. The two distributions are in close agreement. In the particle model, 5×10^4 particles (grid spacing 0.005) are required to reduce the fluctuations in ion density to a sufficiently low level for numerical stability. The kinetic model requires a grid spacing of 0.02. Thus, the kinetic model runs approximately a factor of 16 more quickly, requiring minutes rather than hours to complete the calculation on an ordinary personal computer.

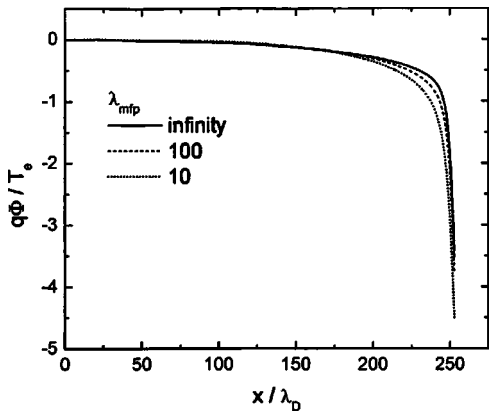

FIG. 4. The potential profile with mean free paths of $10\ \lambda_D$, $100\ \lambda_D$, and infinity. The ionization rates are adjusted to have a plasma extent of $252.8\ \lambda_D$.

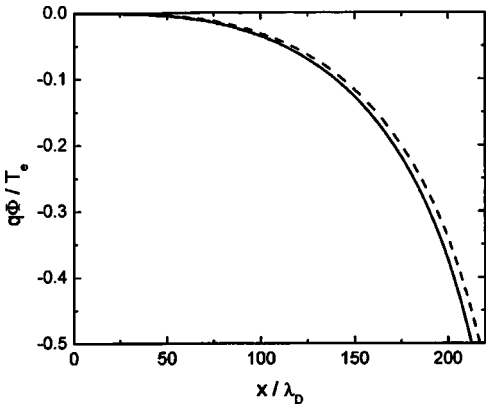

FIG. 5. The potential profile for the quasineutral region for the collisional case $\tilde{\lambda}_{mfp}=5$ (solid line) and the analytic solution, Eq. (14) (dashed line).

Figure 8 is a logarithmic plot of the potential as a function of distance. This plot shows clearly the expected parabolic dependence of the potential profile in the collisionless limit. In the collisional limit, the sheath profile has approximately the expected cubic dependence except near the midplane, where the profile is between parabolic and cubic. This is a consequence of the drift velocity not being correctly described by the high field mobility, Eq. (10), for distances from the midplane that are not large in comparison with the mean free path. Note that the electric field value in the collisional limit, $\tilde{E}_{0.5}=2.58/\tilde{x}_{0.5}$, is not significantly different from that in the collisionless limit, $\tilde{E}_{0.5}=2.64/\tilde{x}_{0.5}$.

IV. SUMMARY AND CONCLUSION

Numerical solutions to a kinetic model for the plasma-sheath problem have been obtained for both collisional and collisionless plasmas. Numerical difficulties at the midplane are removed by having a short initializing region in which

TABLE IV. Comparison of parameters at $\tilde{\Phi}=-0.5$ from the numerical model to the parameters calculated from the analytic model, Eqs. (16)–(18) for the collisional case. The value from the analytic model is given first and the value from numerical model is given second. The values converge as the mean free path is made shorter. The first two columns are the input values for the two models.

Input parameters		Analytic value/value from the model		
λ_{mfp}	$\tilde{R}_0\times10^3$	$\tilde{x}_{0.5}$	$\tilde{E}_{0.5}$	$\tilde{J}_{0.5}$
200	1.74	342/225	0.0075/0.011	0.595/0.391
100	1.55	293/222	0.0088/0.011	0.454/0.346
50	1.32	259/220	0.010/0.012	0.342/0.289
20	0.973	234/217	0.011/0.012	0.227/0.210
10	0.737	223/215	0.012/0.012	0.165/0.158
5	0.543	217/213	0.012/0.012	0.118/0.115

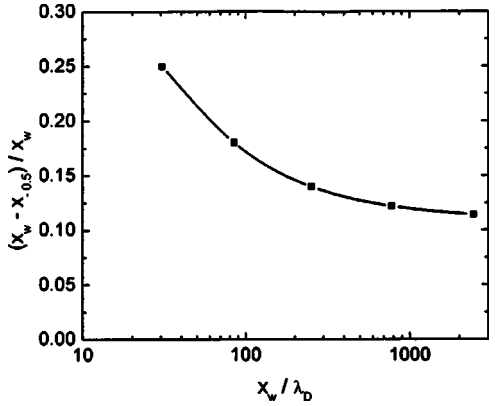

FIG. 6. A plot of the relative distance $(\tilde{x}_w - \tilde{x}_{0.5})/\tilde{x}_w$ as a function of $\tilde{x}_w$ for different plasma sizes and constant collisionality, $L/\lambda_{mfp} = 10$. This shows that the fraction of the discharge that is not quasineutral becomes smaller as the plasma is made larger.

the potential profile is approximated by a polynomial with coefficients chosen to minimize the error in Poisson's equation. The solutions for the quasineutral region in the collisionless case agree with the quasineutral analytic solution of

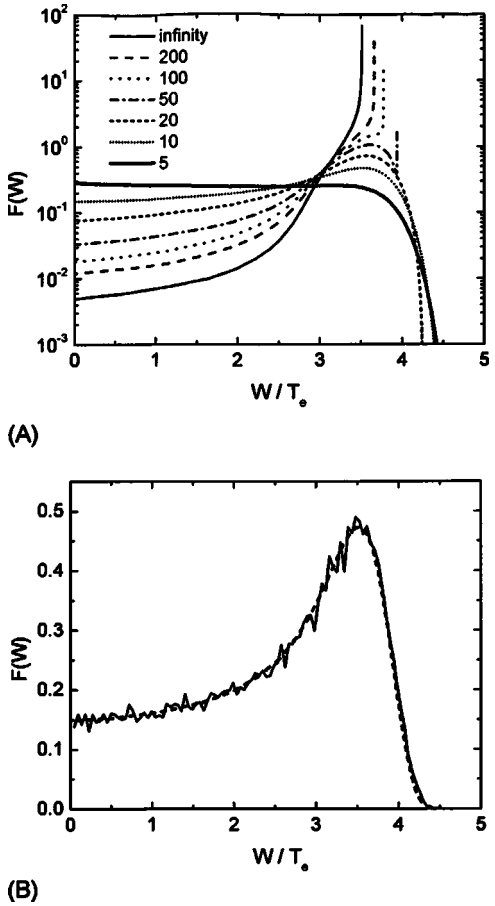

FIG. 7. (A) The energy distribution of ions hitting the wall for different mean free paths. The area of the curves are normalized to unity. (B) Comparison of the energy distribution from the kinetic model (dashed line) to the energy distribution from the particle model (solid line).

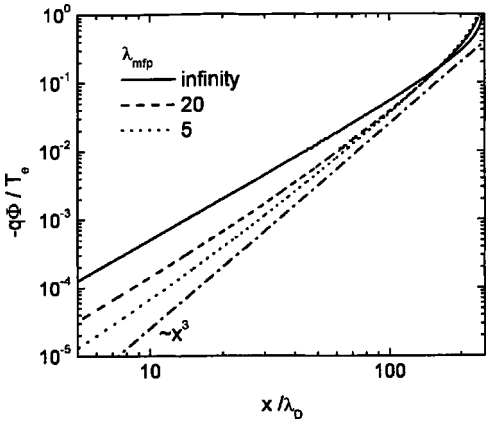

FIG. 8. Logarithmic plot of the potential as a function of distance. Within the quasineutral region, the dependence changes from parabolic in the collisionless case to nearly cubic in the case of short mean free path. The dependence within about a mean free path of the origin shows less change. The slope for infinite mean free path is very nearly 2.0 in the quasineutral region. A slope of 3.0 is plotted for comparison with the collisional case.

Harrison and Thomson [6] except for the smallest plasma sizes studied. The calculated values for $\tilde{n}_i$, $\tilde{J}$, and $\tilde{E}$ are very near to their values from the quasineutral model to the distance for which $\tilde{\Phi} = -0.5$.

The effect of collisions on the potential profile is to round off the knee in the potential profile. The calculated potential profiles in the quasineutral region fall slightly more rapidly with distance than Riemann's analytic solution [3] for this region. The ion flux at the wall is reduced, which requires a more negative wall potential to equalize the electron and ion fluxes. The smaller ion flux also results in a lower ionization rate being required for a given plasma density. The flux is reduced by approximately a factor of 2 when there are 10 mean free paths from the plasma midplane to the wall. The electric field and the flux from the midplane to the point where $\tilde{\Phi} = -0.5$ can be calculated from simple formulas that become accurate to a few percent in the limit of 50 or more mean free paths in the plasma. In the collisionless case, the energy distribution of ions at the wall is peaked at the energy corresponding to the wall potential. As the mean free path becomes shorter, these highest energy ions from near the midplane are removed from the distribution and the peak is shifted to lower energy.

ACKNOWLEDGMENT

This work was supported by the United States Department of Energy through the Plasma Science Initiative.

APPENDIX: NUMERICAL TECHNIQUES

The expression for the ion density, Eq. (4), involves an integral with a singularity that must be handled carefully. The integral is evaluated for the short intervals between grid-points, and these values are summed from the midplane to x. For the interval between adjacent grid points a and b, an approximate analytic expression is used

$$\int_a^b \frac{\tilde{S}(\xi)}{\sqrt{2}[\tilde{\Phi}(\xi)-\tilde{\Phi}(\tilde{x})]^{1/2}}d\xi \cong \frac{\tilde{S}[(a+b)/2]}{\sqrt{2}}\int_a^b \frac{d\tilde{\Phi}(\xi)}{[\tilde{\Phi}(\xi)-\tilde{\Phi}(\tilde{x})]^{1/2}}\frac{d\xi}{d\tilde{\Phi}(\xi)}$$

$$\cong \sqrt{2}\tilde{S}[(a+b)/2]\{[\tilde{\Phi}(b)-\tilde{\Phi}(\tilde{x})]^{1/2}-[\tilde{\Phi}(a)-\tilde{\Phi}(\tilde{x})]^{1/2}\}\left\{\left.\frac{d\Phi(\xi)}{d\xi}\right]_{\xi=(a+b)/2}\right\}^{-1}, \quad \text{(A1)}$$

which removes the singularity, where

$$\tilde{S}(\xi)=\tilde{R}_0(1+\xi/\tilde{\lambda}_{mfp})\exp[-(\tilde{x}-\xi)/\tilde{\lambda}_{mfp}], \quad \text{(A2)}$$

and $\xi=(a+b)/2$. Thus, $\tilde{S}(\xi)$ is evaluated at the midpoint of the interval. Both $\tilde{S}(\xi)$ and $d\tilde{\Phi}/d\xi$ are assumed to change negligibly on the interval and are taken through the integral sign. This assumption requires $(b\text{-}a)/\lambda_{mfp}\ll 1$, which is satisfied by the small grid spacing. The integral over the whole domain is obtained by summing the right-hand side for each pair of adjacent grid points, with the approximation

$$\left.\frac{d\Phi(\xi)}{d\xi}\right|_{\xi=(a+b)/2} \cong \frac{\Phi(b)-\Phi(a)}{b-a}. \quad \text{(A3)}$$

This is, in effect, the value of the derivative at the midpoint. The accuracy of Eq. (A1) was examined by using a fourth-order polynomial for $\tilde{\Phi}(\tilde{x})$ and comparing the numerical result for the integral with a more precise result obtained with a finer grid. The error was found to be less than of order 10^{-6} with 100 grid points on the interval. A high level of accuracy is needed because the integration of Poisson's equation depends upon the small difference between the electron and ion densities which is of order $(\lambda_D/L)^2$. The accuracy is insufficient if the number of terms in the sum is too small. An initializing interval of 0.15 L was found to give a sufficiently large number of terms. The sum over previous points results in the computation time scaling as the square of the number of grid points.

Poisson's equation is integrated using the second-order relation [14]

$$\tilde{\Phi}(\tilde{x}_{k+1})=2\tilde{\Phi}(\tilde{x})-\tilde{\Phi}(\tilde{x}_{k-1})-(\Delta\tilde{x})^2[\tilde{n}_i(\tilde{x}_k)-\tilde{n}_e(\tilde{x}_k)]. \quad \text{(A4)}$$

A very small step size, $\leqslant 0.05$, is necessary to avoid numerical instability with either this second-order method or with fourth-order Runge-Kutta. The small step size makes the second-order method sufficiently accurate. If fourth-order Runge-Kutta is used, there is a need to evaluate the integral for $n_i(x)$ within the derivatives subroutine and Δx takes on half the usual value in two of the four evaluations of the derivative. The fourth-order method is thus more complicated and does not offer an advantage in step size because this is limited by numerical stability. The fourth-order method was implemented for a few cases, and the values found for $\tilde{x}_w$ (for example) differed by only a few percent from values obtained from the second-order method.

For the particle model, sufficient accuracy for the density requires that the ions be given an average velocity calculated for the region between the gridpoint at the birth location and the next grid point. The average defined by

$$v_{i,k}=\frac{1}{2}\left[\sqrt{\frac{2q}{m_i}[\Phi(x_i)-\Phi(x_k)]}+\sqrt{\frac{2q}{m_i}[\Phi(x_{i+1})-\Phi(x_k)]}\right], \quad \text{(A5)}$$

gives a value for density contribution that is sufficiently accurate.

[1] K.-U. Riemann, Phys. Fluids **24**, 2163 (1981).
[2] L. Tonks and I. Langmuir, Phys. Rev. **34**, 876 (1929).
[3] K.-U. Riemann, Phys. Plasmas **4**, 4158 (1997).
[4] C. K. Birdsall, IEEE Trans. Plasma Sci. **19**, 65 (1991).
[5] R. T. Farouki, S. Hamaguchi, and M. Dalvie, Phys. Rev. A **44**, 2664 (1991).
[6] E. R. Harrison and W. B. Thomson, Proc. Phys. Soc. London **74**, 145 (1959). This reference and Ref. [6] use $\sqrt{2T_e/m_i}$ to generate the dimensionless units rather than $\sqrt{T_e/m_i}$; thus, the dimensionless distances correspond to $\tilde{R}\tilde{x}/\sqrt{2}$.
[7] S. A. Self, Phys. Fluids **6**, 1762 (1963).
[8] P. C. Stangeby, Phys. Fluids **27**, 682 (1984).
[9] L. A. Schwager, Phys. Fluids B **5**, 631 (1993).
[10] G. H. Wannier, Phys. Rev. **83**, 281 (1951).
[11] G. H. Wannier, *Statistical Physics* (Dover, New York, 1987), Chaps. 18 and 21.
[12] B. M. Smirnov, *Physics of Weakly Ionized Gases* (Mir, Moscow, 1981), p. 217.
[13] S. Robertson and Z. Sternovsky, Phys. Rev. E **67**, 046405 (2003).
[14] L. Verlet, Phys. Rev. **159**, 98 (1967).